PHYSICAL REVIEW B **88**, 155319 (2013)

Excitonic fine structure of elongated InAs/InP quantum dots

M. Zieliński*

Institute of Physics, Faculty of Physics, Astronomy and Informatics, Nicolaus Copernicus University, Grudziadzka 5, 87-100 Torun, Poland

(Received 19 August 2013; revised manuscript received 25 September 2013; published 22 October 2013)

The bright exciton splitting in nanosystems and its origins are of primary importance for quantum-dot-based entangled-photon-pair generation. In this paper, I investigate excitonic energies and fine structure for million-atom InAs/InP quantum dots using many-body theory in conjunction with the empirical tight-binding method. Whereas the phenomenological theories relate the fine-structure splitting to quantum-dot-shape asymmetry, using an atomistic approach I demonstrate that for certain elongated quantum-dot shapes the bright exciton splitting can be significantly reduced. I demonstrate that strain effects play an essential role as the main contribution to the bright exciton splitting in InAs/InP quantum dots and observe highly reduced fine-structure splitting for high-symmetry quantum dots without wetting layer. I report the "intrinsic" fine-structure splitting, due to the underlying crystal lattice, to be generally significantly larger than the values predicted by the empirical pseudopotential calculations. Finally, I study excitonic properties of alloyed InAsP quantum dots and demonstrate that alloying effects can significantly reduce fine-structure splitting even in significantly elongated quantum dots.

DOI: 10.1103/PhysRevB.88.155319 PACS number(s): 73.21.La, 73.22.−f, 78.67.Hc, 03.67.Bg

Various potential applications in quantum cryptography[1] and quantum computations[2] necessitate efficient entangled-photon-pair generation. The biexciton-exciton cascade process in semiconductor quantum dots (QDs) has been proposed as a source of polarization entangled photon pairs,[3] yet for realistic QDs the intermediate exciton state is split by the electron-hole exchange interaction.[4] The energetic difference between the two bright exciton states, known as the fine-structure splitting (FSS), is typically (10–100 μeV) much larger than the radiative linewidth (1 μeV), hindering the process of entangled-photon-pair generation.

There are ongoing experimental efforts to manipulate and reduce the FSS including the post-growth annealing techniques,[5] spectral filtering,[6] the selection ("cherry picking") of QDs with low FSS,[7] or the site-controlled growth of high-symmetry pyramidal QDs.[8] On the other hand, the dynamic control of the FSS involves application of electric[9,10] and magnetic fields,[11] dressing excitons with photons,[12] applying stress,[13,14] or the simultaneous application of two fields, e.g., large strain and electric fields.[15]

The FSS is also a subject of intensive theoretical research. Whereas the "effective" theories[4,16,17] relate the FSS to the QD-shape asymmetry, recent atomistic calculations emphasize the role of the true atomistic symmetry due to the underlying zinc-blende lattice.[14,18–21] In an atomistic calculation, the bright exciton splitting is therefore present even in fully shape-symmetric dots, where the standard $\mathbf{k}\cdot\mathbf{p}$ theory predicts no FSS (Refs. 16 and 17) and requires sophisticated symmetrization[22–24] to account for the correct atomistic symmetry. It is therefore convenient to decompose[25] the FSS into the "extrinsic" contribution due the QD macroscopic shape anisotropy or elongation[26] and the "intrinsic" FSS due the crystal lattice, that can be present even in shape-symmetric QDs.

Although recent theoretical efforts focus on development of the group-theoretical interpretation of the FSS, a detailed quantitative understanding of the FSS is still lacking. For example, in this paper I study a large set of QDs having the same point-group symmetry, yet with the FSS values spanning two orders of magnitude. I demonstrate that the strain effects are predominantly responsible for the magnitude of the intrinsic FSS and I also study effects of alloying. Further, I report the FSS values significantly larger then those predicted by the empirical pseudopotential method (EPM). As noticed by the EPM researchers,[27] this method systematically predicts much lower FSS values than those reported in the experiment (or in the current empirical tight-binding paper). I do not confirm highly reduced FSS for InAs/InP systems as predicted by the EPM,[25] nor the necessity of the "ordering effects" inclusion[27] for the theoretical explanation of the observed FSS values.

I. METHODS

The calculation consists of several major steps: first atomic positions are calculated. To calculate strain-relaxed positions, I use the atomistic valence force field (VFF) approach of Keating.[28] This method is described in more detail in Refs. 29 and 30 and in our previous papers.[31–34] To preserve the axial symmetry of QDs, I model the external InP (or GaAs) buffer surrounding QDs as a cylinder (see Fig. 1). The computational domains for the strain calculation (96 nm diameter and 120 nm height) have reached over 30 million atoms.[35] For all considered QD systems, the size of the computational domain guarantees convergence of the strain distribution.[35]

Due to the small lattice mismatch of InAs and InP, I neglect the piezoelectric effects in the present calculation, following similar arguments by Gong *et al.*[36] who ignore piezoelectricity in the empirical pseudopotential paper on InAs/InP quantum dots. Consistently, piezoelectric effects can generally be neglected for low-aspect-ratio[37–39] quantum dots, such as studied in this paper, for which the piezoelectricity is either negligible[40] or the contribution due to second-order effects tends to cancel linear terms.[37,41]

Once the atomic positions of the strained system are obtained, I use them to calculate single-particle energies with the empirical tight-binding model that accounts for strain, d orbitals, spin-orbit interactions, and for the atomistic effects such as the dot/matrix interface and crystal-lattice symmetry.[33,34]

The single-particle tight-binding Hamiltonian for the system of N atoms and m orbitals per atom can be written, in the

language of the second quantization, in the following form:

$$\hat{H}_{\mathrm{TB}} = \sum_{i=1}^{N}\sum_{\alpha=1}^{m} E_{i\alpha} c_{i\alpha}^{+} c_{i\alpha} + \sum_{i=1}^{N}\sum_{\alpha=1,\beta=1}^{m} \lambda_{i\alpha,\beta} c_{i\alpha}^{+} c_{i\beta} + \sum_{i=1}^{N}\sum_{j=1}^{4}\sum_{\alpha,\beta=1}^{m} t_{i\alpha,j\beta} c_{i\alpha}^{+} c_{j\beta}, \quad (1)$$

where $c_{i\alpha}^{+}$ ($c_{i\alpha}$) is the creation (annihilation) operator of a carrier on the orbital α localized on the site i, $E_{i\alpha}$ is the corresponding onsite (diagonal) energy, and $t_{i\alpha,j\beta}$ describes the hopping (off-site, off-diagonal) of the particle between the orbitals on (4) nearest-neighboring sites. Coupling to further neighbors is neglected. Finally, $\lambda_{i\alpha,\beta}$ (onsite, off-diagonal) accounts for the spin-orbit interaction following the description given by Chadi.[42]

Strain in the tight-binding (TB) method is accounted by the modification of Hamiltonian matrix elements from bulk (unstrained) values to values modified due to bond lengths/angles modification. Therefore, for the case with strain effects (artificially) neglected, I use bulk TB parameters set from Ref. 43 and there is no strain contribution in the Hamiltonian nor the relaxation of atomic positions is accounted for. It should, thus, be emphasized that if one uses InAs/InP bulk Hamiltonian matrix elements, one is simply neglecting strain effects. For the strained systems, since strain effects change bond lengths and angles, strain-relaxed positions are used to modify TB parameters (diagonal and off-diagonal matrix elements) following the description given in detail in my earlier paper.[33]

Coulomb matrix elements (Coulomb direct and exchange integrals) are calculated according to the approach given in Ref. 32. In this approach, not being able to calculate the effective Coulomb interaction self-consistently,[44] one assumes a statically screened Coulomb interaction. Hence, the Coulomb matrix elements V_{ijkl} are given by

$$V_{ijkl} = \iint \phi_i^{*}(\vec{r}_1)\phi_j^{*}(\vec{r}_2)\frac{e^2}{\epsilon(\vec{r}_1,\vec{r}_2)|\vec{r}_1-\vec{r}_2|}\phi_k(\vec{r}_2)\phi_l(\vec{r}_l), \quad (2)$$

where $\epsilon(\vec{r}_1,\vec{r}_2)$ is the position-dependent dielectric function and ϕ are single-particle wave functions. The tight-binding wave function is given in the form of linear combination of atomic orbitals (LCAO):

$$\phi_i = \sum_{\vec{R},\alpha} b_{\vec{R}\alpha}^{i} |\vec{R}\alpha\rangle, \quad (3)$$

where $\vec{R}\alpha$ is the α orbital localized on atom $\vec{R}$, and $b_{\vec{R}\alpha}^{i}$ is the LCAO expansion coefficient. By substituting Eq. (3) into Eq. (2) and then by utilizing a series of approximations,[32,45] one gets an approximate form of Coulomb matrix elements[32]

$$V_{ijkl} = \sum_{\vec{R}_1}\sum_{\vec{R}_2\neq\vec{R}_1}\left[\sum_{\alpha_1} b_{\vec{R}_1\alpha_1}^{i*} b_{\vec{R}_1\alpha_1}^{l}\right]\left[\sum_{\alpha_2} b_{\vec{R}_2\alpha_2}^{j*} b_{\vec{R}_2\alpha_2}^{k}\right] \times \frac{e^2}{\epsilon|\vec{R}_1-\vec{R}_2|} + \sum_{\vec{R}_1}\sum_{\alpha_1\alpha_2\alpha_3\alpha_4} b_{\vec{R}_1\alpha_1}^{i*} b_{\vec{R}_1\alpha_2}^{j*} b_{\vec{R}_1\alpha_3}^{k} b_{\vec{R}_1\alpha_4}^{l} \times \langle\vec{R}_1\alpha_1,\vec{R}_1\alpha_2|\frac{e^2}{|\vec{r}_1-\vec{r}_2|}|\vec{R}_1\alpha_3,\vec{R}_1\alpha_4\rangle, \quad (4)$$

where α is the orbital index and $\vec{R}_i$ denotes the position of the ith atom.

The first term is the long-range, bulk-screened, contribution to the two-center integral built from the monopole-monopole interaction[46,47] of two charge densities localized at different atomic sites. The second term is the onsite unscreened part, calculated by direct integration using atomic (Slater) orbitals.[48,49] This approach is justified by the fact that the screening (Thomas-Fermi) radius (≈2–4 Å) is on the order of bond length[49,50] resulting in the nearly bulk screening of off-site (long-range) terms and limited screening of onsite (short-range) contribution.

By using a multiscale[35] approach, the number of atoms for the single-particle calculation is reduced. Both the single-particle (tight-binding) and Coulomb matrix elements calculations domains[35] contained ≈1 million atoms. The Hamiltonian for the interacting electrons and holes can be written in second quantization as[51]

$$\hat{H}_{\mathrm{ex}} = \sum_i E_i^e c_i^{\dagger} c_i + \sum_i E_i^h h_i^{\dagger} h_i + \frac{1}{2}\sum_{ijkl} V_{ijkl}^{ee} c_i^{\dagger} c_j^{\dagger} c_k c_l + \frac{1}{2}\sum_{ijkl} V_{ijkl}^{hh} h_i^{\dagger} h_j^{\dagger} h_k h_l - \sum_{ijkl} V_{ijkl}^{\mathrm{eh,dir}} c_i^{\dagger} h_j^{\dagger} h_k c_l + \sum_{ijkl} V_{ijkl}^{\mathrm{eh,exchg}} c_i^{\dagger} h_j^{\dagger} c_k h_l. \quad (5)$$

The many-body Hamiltonian for the electron-hole pair (exciton) is solved using the configuration interaction approach.[32,52] The excitonic Hamiltonian does include vertex corrections[44] in the form of electron-hole interaction, but self-energy corrections are included indirectly in the electron and hole energies fitted to experimental transitions of bulk material. The contribution to the self-energy correction due to the presence of image charges at the quantum dot/surrounding interface is small primarily because of cancellation between the self-energy interaction of each particle with its own image charges and the excitonic corrections.[53]

Typically,[4] excitonic fine structure is calculated using a basis formed by the lowest-electron and -hole states only. In this paper, however, for the configuration interaction calculations, following Ref. 19, I use all possible determinants constructed from the 12 lowest-energy electron and 12 lowest-hole states (including spin). Finally, the optical spectra are found by calculating the intensity of photoluminescence from the recombination of one electron-hole pair in an N-exciton state using Fermi's golden rule:[32,51,52]

$$I(\omega) = \sum_f |\langle f,N-1|P^{-}|i,N\rangle|^2 \delta(E_i - E_f - \hbar\omega), \quad (6)$$

where $|i,N\rangle$ is ith state of the N-exciton system and $\langle f,N-1|$ is fth state of the $N-1$ exciton. The interband polarization operator P^{-} describes all the possible electron-hole recombination channels:[51]

$$P^{-} = \sum_{lm} \langle l_e|\vec{\epsilon}\cdot\vec{r}|m_h\rangle c_l h_m, \quad (7)$$

where $\langle l_e|\vec{\epsilon}\cdot\vec{r}|m_h\rangle$ is a dipole matrix element[45] calculated from single-particle (electron and hole) tight-binding wave

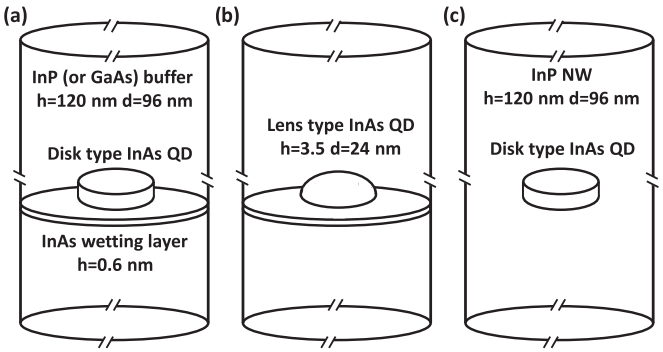

FIG. 1. Schematics of quantum-dot shapes and computational domains (see the text) considered in the paper: (a) disk-shaped InAs QD on a InAs wetting layer surrounded by a InP or GaAs buffer, (b) lens-shaped InAs QD on a InAs wetting layer surrounded by a InP or GaAs buffer, and (c) disk-shaped QD without the wetting layer, a nanowire QD.

functions for a given polarization of light $\vec{\epsilon}$. In this work, I consider only single excitons and identical occupation probability of both bright excitonic states (corresponding to low-pumping power and low-temperature limit in the experiment). In the case of a single exciton, the above equations are further simplified with the final state being the vacuum.

II. RESULTS

I have studied a large family of over 300 different InAs/InP QDs. Several InAs/GaAs systems have been investigated as well for comparison. I start with the results for the disk-shaped InAs/InP QD similar to those grown by the indium-flush self-assembly approach.[54] The QD height is 3 nm and the diameter is 20.6 nm. The QD is localized on a 0.6-nm-thick wetting layer (Fig. 1). The presence of the wetting layer is particularly important for disk-type quantum dots as it lowers the overall quantum-dot symmetry from D_{2d} to C_{2v} (the lack of "rotoinversion operation"[19]), and therefore disk-type quantum dots located on the wetting layer have low C_{2v} symmetry. The lateral shape of the QD is modified from cylindrical to elliptical (Fig. 2), with the anisotropy parameter t defining lengths of the major $x = r \times (1 + t)$ and minor $y = r/(1 + t)$ QD axes, with r being the radius of the cylindrical ($t = 0$) QD. I consider the elongation along two nonequivalent [110] and [1$\underline{1}$0] crystal axes.[19,26]

Figure 3 shows the evolution of the single particle: (a) electron and (b) hole levels as a function of the QD-shape anisotropy. As the deformation keeps the volume of the QD fixed, and thus the overall confinement, both the ground electron (e_1) and the ground hole (h_1) state energies do not change significantly with the shape deformation, even for the largest considered anisotropy $|t| = 0.2$. The decreased confinement along the longer QD's axis is compensated by the increased confinement along the shorter of the axes. The excited, higher-angular-momentum [p shell: e_2 and e_3, Figs. 2 and 3(a)] electron states are more susceptible to the shape deformation. The underlying lattice asymmetry[40] leads to the p-shell ($e_3 - e_2$) splitting (1.6 meV) even when the macroscopic quantum-dot shape is cylindrical ($t = 0$). For the elongation along [1$\underline{1}$0], the p-shell splitting is further

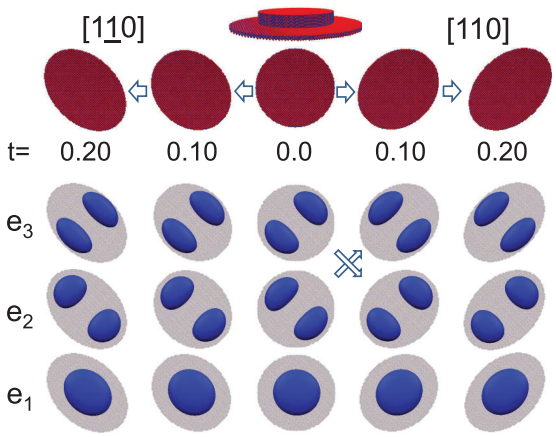

FIG. 2. (Color online) Upper row: schematics of a shape deformation applied to a InAs/InP disk-shaped QD (see the text) along inequivalent [110] and [1$\underline{1}$0] crystal axes. The deformation parameter t defines the major $x = r \times (1 + t)$ and minor $y = r/(1 + t)$ axes of an elongated QD. Lower rows: single-particle probability density isosurfaces for several lowest-electron states as a function of InAs/InP disk-shaped QD deformation.

increased. However, the [110] elongation counters the asymmetry due to the zinc-blende lattice, leading to the reduced p-shell splitting for $t \approx 0.015$ [Fig. 3(a)] and the apparent crossing of the p levels (Fig. 2).

The hole states, due to higher effective mass and better confinement, are less susceptible to the shape deformation [Fig. 3(b)]. The hole p-shell splitting (≈2 meV) and splittings of the higher-lying shells remain less affected even for the highest considered anisotropy and show little difference with respect to the choice of the deformation axis. Although I present results for a specific QD, all the above conclusions can be generalized for InAs/InP disk-shaped QDs of different sizes.

Next, I study many-body, excitonic properties for a family of InAs/InP disk-type quantum dots of the same height (3 nm) and different diameters. I have carried out extensive calculations of the excitonic properties for 278 different InAs/InP QDs. Figure 3(c) shows the evolution of the excitonic band gap under QD-shape deformation. As expected from the quantum confinement effect, the energy of the exciton decreases with the increasing QD diameter. The excitonic gap is given by contributions due to single-particle gap (≈740–770 meV) and the electron-hole $J_{\rm eh} \equiv V_{e_1h_1h_1e_1} = \iint \frac{|e_1(r)|^2|h_1(r')|^2}{\epsilon(r,r')|r-r'|}$ Coulomb attraction (≈20–24 meV), i.e., $E_X \approx E_{sp} - J_{\rm eh}$. There is also a small (≈ -1 meV) correction due to the correlation effects. The excitonic band gap does not vary significantly with the deformation and there is virtually no difference between the two nonequivalent elongation axes. The difference between a cylindrical and deformed system lies within several meV range and is mostly due to a small increase in the single-particle gap, whereas the electron-hole Coulomb attraction remains almost unaffected by the deformation: a hallmark of a long-range character of the direct Coulomb interaction. Figure 3(d) shows the evolution of the bright-dark exciton splitting, being predominately given by the electron-hole exchange integral $K_{\rm eh} \equiv V_{e_1h_1e_1h_1} = \iint \frac{e_1^*(r)h_1^*(r)e_1(r')h_1(r')}{\epsilon(r,r')|r-r'|} dr\, dr'$. The

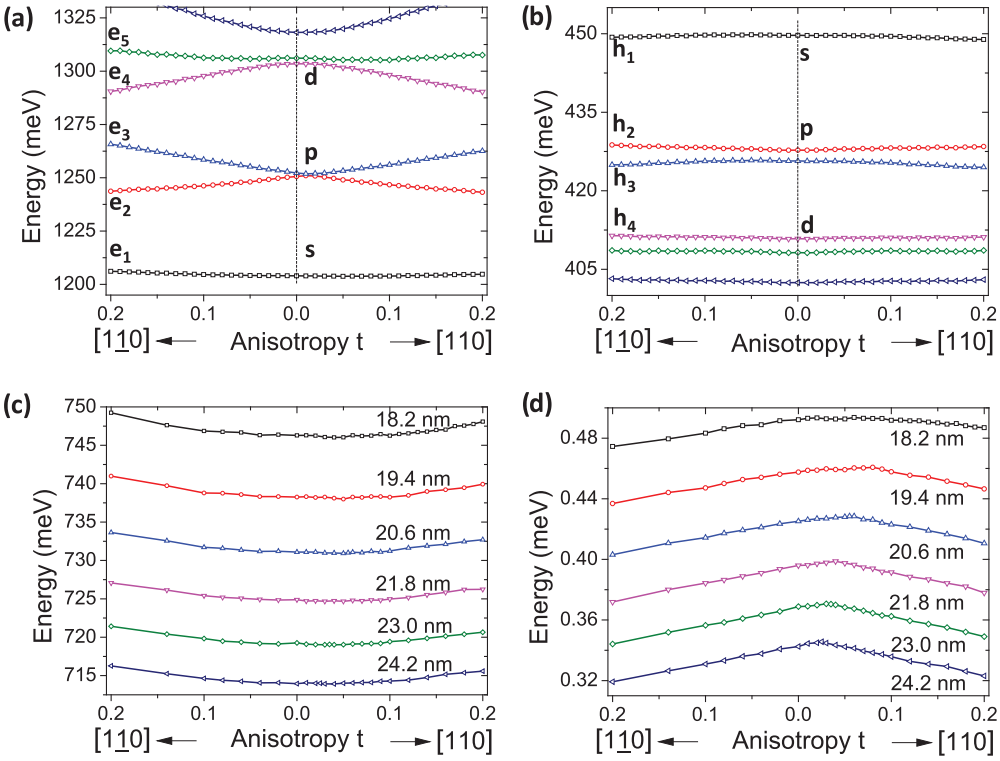

FIG. 3. (Color online) Evolution of the single particle: (a) electron and (b) hole levels; (c) the excitonic band gap and (d) the bright-dark exciton splitting (electron-hole exchange splitting) as a function of InAs/InP disk-shaped QD deformation t along inequivalent [110] and [1$\bar{1}$0] crystal axes. (a) and (b) are calculated for QD of $h = 3.0$ nm and $D = 20.6$ nm, whereas (c) and (d) are calculated for a family of QD systems of the same height (3.0 nm) and different diameter. Lines connect and order states energetically.

electron-hole exchange is indirectly related to the spatial overlap of the electron and hole states, thus it is larger for smaller (or better confined) QDs. The bright-dark exciton splitting for the larger-diameter QD varies more significantly with the shape deformation and reveals more pronounced difference with respect to the choice of the elongation axis. Yet, in general, there is a relatively small difference of the bright-dark exciton splitting between elongated and cylindrical QDs.

Further, I investigate the "anisotropic" electron-hole exchange[4] resulting in the splitting of the bright excitonic doublet. Figure 4(a) shows the evolution of the bright exciton splitting as a function of the QD-shape deformation for the same family of InAs/InP QDs as studied on Figs. 3(a) and 3(b). Importantly, for the shape-symmetric system ($t = 0$), there is still a nonzero FSS due to the underlying crystal-lattice asymmetry and the low-C_{2v} total symmetry of the QD.[19] The value of this crystal-lattice-induced ("intrinsic"[25]) splitting varies between 6 and 14 μeV and is larger for smaller diameter QDs, consistent with the increased electron-hole interaction in a smaller nanosystem. With the increasing shape deformation along the [1$\bar{1}$0] crystal axis, the shape ("extrinsic"[25]) anisotropy adds to the splitting due to the crystal lattice and the overall bright exciton splitting is increased, even up to 50 μeV for the largest shape anisotropy and the largest studied QD. However, for the deformation along the [110] crystal axis, the shape anisotropy counteracts the crystal-lattice anisotropy, leading to a highly reduced (well below 1 μeV) bright exciton FSS and the apparent crossing of the two bright excitonic lines.[25] Due to the different slope of the FSS evolution with t, the aspect ratio for which the FSS reduction occurs varies strongly depending on the diameter: $t_{\min} \approx 0.16$ for the $D = 18.2$ nm and dropping exponentially-like to $t_{\min} \approx 0.03$ for the largest considered $D = 24.2$ nm. Thus, the larger-diameter QDs are more susceptible to the shape deformation, with the slope of the FSS evolution being proportional to the QD diameter. I conclude that should the elongation be an important factor, the larger-diameter (low-emission energy) InAs/InP QDs should generally have larger FSS. This is in contradiction to the recent empirical pseudopotential method calculations,[25] yet observed experimentally for different sorts of QDs, e.g., InAs/GaAs (Ref. 56) and GaAs/AlAs (Ref. 26) QDs. Caution should be exercised though: Fig. 4(a) combined with Fig. 3(c) shows that in general there may not be a clear relation between the excitonic energy and the FSS,[10] e.g., for the $t = 0.06$ and the [1$\bar{1}$0] deformation all QDs considered here have the FSS close to $\approx$20 μeV, whereas the emission energies vary in a wide range from 712 to 746 meV. Therefore, a particular relation between the FSS and the exciton energy may be sample depended.

In order to verify the character of the bright excitonic lines crossing, on Fig. 4(b) I show the polarization, the emission intensity, and the FSS for one of the InAs/InP disk-shaped QDs ($h = 3.0$ nm and $D = 20.6$ nm), whereas I have checked that all the conclusions stated here are valid for other considered diameters. For a cylindrical QD shape ($t = 0$), the energetically lower excitonic line is polarized along the

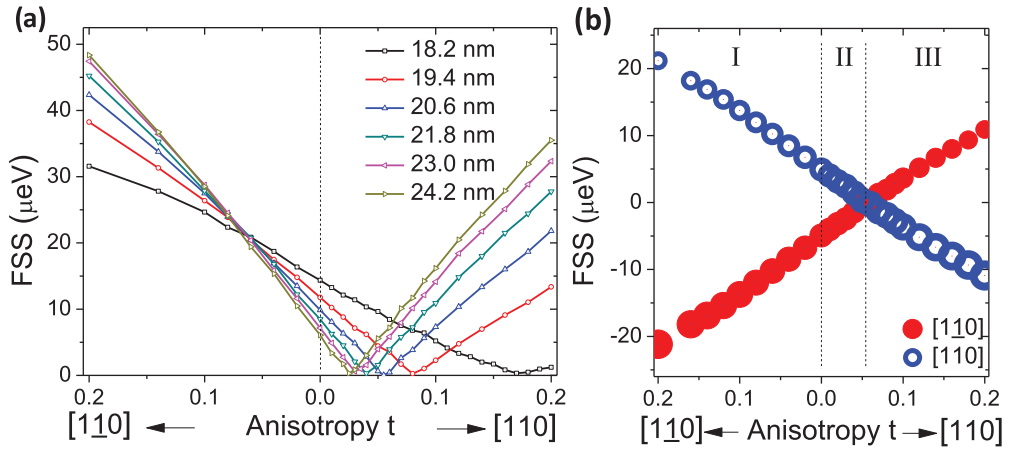

FIG. 4. (Color online) (a) The bright exciton FSS as a function of QD-shape deformation t along two inequivalent crystal axes for a family of InAs/InP disk-shaped QDs of different diameter and equal height ($h = 3.0$ nm); (b) emission intensity, polarization, and the FSS of the two bright excitonic lines for InAs/InP disk-shaped QD ($h = 3.0$ nm and $D = 20.6$ nm). The bright exciton FSS is measured from the center of the excitonic emission. The blue (empty) circles represent the [110] polarized transition, while the red (full) circles represent [1$\bar{1}$0] polarized transitions. The size of the circles is proportional to the oscillator strengths.

[1$\bar{1}$0] axis, whereas, the energetically higher bright exciton line is polarized along the perpendicular [110] direction. When applying the shape deformation (along the [110] axis), for $t \approx 0.055$, the observed FSS drops to a very small, almost degenerate, value of $\approx$0.05 μeV; then with further deformation, one observes the crossing of the two bright lines and reversal of their polarizations.

There are basically three different ranges as denoted on Fig. 4(b): for "I" and "III" the polarization of the lower excitonic line follows the longer axis of the QD and its intensity is larger than that of an energetically higher excitonic line. QDs in the I region are sometimes marked as having the "positive" FSS, whereas QDs in the III" region are denoted as having the "negative" FSS.[10] There is also an another (positive) FSS range (II), where the polarization ordering is anticorrelated with elongation direction: the lower excitonic line follows the shorter (minor) axis of an elongated QD. For comparison, I carried out calculations for an analogous InAs/GaAs disk-shaped system ($h = 3.0$ nm and $D = 20.6$ nm) and found that those QDs always have FSS > 0 and the polarization of the low-energy exciton line is always [1$\bar{1}$0]. Thus, for [110] elongation (and $t \leqslant 0.2$), the polarization of the low-energy exciton is perpendicular to the elongation axis. Such anticorrelation between the FSS and polarization anisotropy has been experimentally observed[56] for InAs/GaAs QDs in agreement with my calculations.

For the configuration interaction, I use all possible determinants constructed from the 12 lowest-energy electron and hole states (spin included). However, as the excitonic ground state is built predominately from electron and hole in their ground s-like state,[4] it could be expected that the contribution from the higher-lying (electron and hole p and d) shells is relatively small. In fact, for cylindrical ($t = 0$) systems, more than about 80% of the FSS magnitude is already accounted for at a level of the contributions from the s shell. Only the 20% of the splitting magnitude can be attributed to configuration mixing effects with higher-lying states. However, for elongated systems, the effect of higher shells is strongly increased and can even dominate over the s-shell contribution, reaching more than $\approx$60% of total fine-structure splitting for the strongly ($t = 0.2$) elongated QDs. It is important to note that although the magnitude of the splitting is strongly increased, the excitonic bright states still have dominant contributions ($\approx$99%) from the electron and hole s shell. This emphasizes the importance of the correlation mixing with large angular momenta states for the quantitative description of the FSS in QDs. I have checked that both the electron and hole p shell should be included in the configuration interaction calculation on equal footing, whereas the contribution from the higher d shell can be safely neglected. With the p shell included, the effective size of the excitonic Hamiltonian is 36×36 rather than the customary 4×4 Hamiltonian including only s-shell contributions.[4]

I emphasize that group-theoretical arguments should always be backed up by a quantitative calculation: in the case of systems considered so far in this paper, the FSS varies within a large range, from 0.1 to 50 μeV, whereas the overall symmetry of considered systems (C_{2v}) is not altered. Another example is demonstrated in Fig. 5, which shows the evolution of the excitonic band gap of a cylindrical

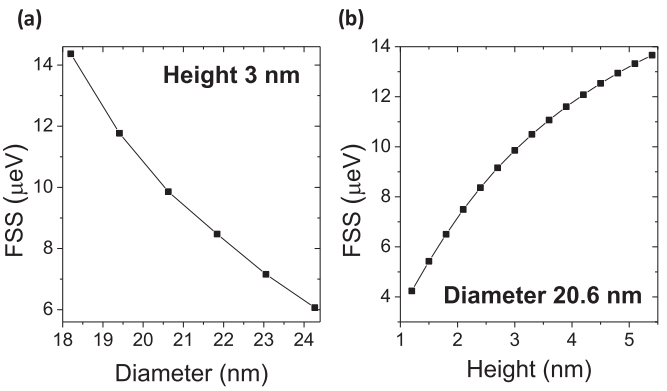

FIG. 5. The bright exciton FSS for a disk-shaped (cylindrical, $t = 0$) InAs/InP QD as a function of (a) QD height or (b) QD diameter.

(not elongated) disk-shaped quantum dot as a function of quantum-dot diameter (a) and height (b). As discussed earlier, the FSS is reduced with the increasing quantum-dot diameter due to decreased electron-hole interaction in a less-confined system. Interestingly, one observes an opposite trend with the increasing quantum-dot height and keeping the diameter fixed. This can be understood as follows: increased quantum-dot height leads to increased light-hole contribution[18,55] to the ground hole state. This will further contribute to FSS due to the exchange interaction coupled via the light-hole admixture.[56,57] The above observation should be important for tailoring quantum-dot properties by engineering quantum-dot height.[58] Additionally, it demonstrates that from the theoretical point of view, only multiband calculations capturing the real symmetry of the system are capable of qualitatively predicting the details of the excitonic spectra.

A. Strain effects and the wetting layer

It was recently found[31,40] that the QD electronic structure can be studied in terms of the contributions from atomic interfaces and strain effects separately. In this spirit, I study the FSS by artificially neglecting the strain effects, i.e., by assuming the strain unrelaxed atomic positions, although not affecting the overall C_{2v} symmetry of the system. Figure 6(a) shows the evolution of the bright exciton splitting as a function of the QD-shape deformation for the same family of disk-type InAs/InP QDs as studied above, yet with strain effects neglected. For $t = 0$, the FSS is nonzero, yet significantly reduced (well below $\approx 0.2\ \mu$eV) and is increasing with the increasing shape elongation, whereas there is virtually no difference with respect to the choice of the elongation axis. The slope of the FSS evolution with respect to the deformation is slightly larger for smaller-diameter nanosystems, but generally comparable for all considered diameters. This is in contrary to the case with the strain effects included, where there is a strong dependence of the FSS slope on the quantum-dot diameter. Figure 6(a) demonstrates that, apart from symmetry considerations, strain effects play an essential role as the main, quantitative contribution to the bright exciton splitting in disk-shaped InAs/InP quantum dots.

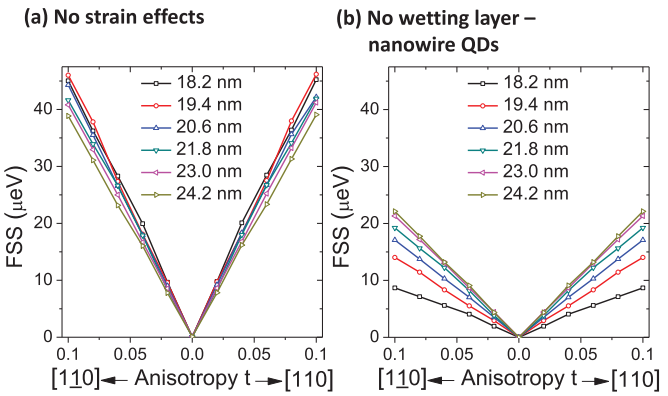

FIG. 6. (Color online) The bright exciton FSS as a function of QD-shape deformation t along two inequivalent crystal axes for a family of InAs/InP disk-shaped QDs of different diameter and equal height ($h = 3.0$ nm). (a) Strain effects have been neglected or (b) the presence of the wetting layer has been neglected.

In a similar way, I estimate the contribution of the wetting layer to the FSS. The wetting layer has a relatively small influence on the absolute value of the excitonic emission, as it reduces the excitonic gap by 5% due to the effective increase of the QD height (confining-potential width[59]). More importantly, with the wetting layer artificially removed, the QD symmetry is higher[19] and equal to that of the zinc-blende [001] grown nanowire QDs.[64] By symmetry, such a system should have exactly zero FSS for a shape-cylindrical $t = 0$ case, as confirmed by my atomistic calculation [Fig. 6(b)]. The dependence of the FSS on the elongation is nearly linear and is strongly influenced by the quantum-dot diameter. I conclude that the presence of the wetting layer induces the vertical inversion anisotropy significantly affecting the FSS.

Next, I study the polarization anisotropy of the excitonic transition for the elongated disk-shaped InAs/InP systems (Fig. 7), defined as $P = |\frac{I_{[110]} - I_{[1\bar{1}0]}}{I_{[110]} + I_{[1\bar{1}0]}}| \times 100\%$, where I_{110} and $I_{1\bar{1}0}$ are the intensities of excitonic emission (summed over both bright states) polarized along the [110] and [1$\bar{1}$0] axes.

In the case with strain effects included, there is a nonzero $\approx$2% polarization anisotropy even in a fully cylindrical system [Fig. 7(a)]. Interestingly, the polarization anisotropy is not correlated with the FSS. The FSS minimum occurs for the [110] elongation, whereas the polarization anisotropy reaches minimum for a relatively small $t \approx 0.01$ elongation along the [1$\bar{1}$0] direction. This value is similar for all considered disk-shaped QD diameters. As the excitonic intensities (related to decay rates) affect the quality ("concurrence") of the entanglement,[60] the large difference of both excitonic bright line intensities (thus high-polarization anisotropy) might in principle affect the degree of the entanglement even in systems with the FSS reduced.

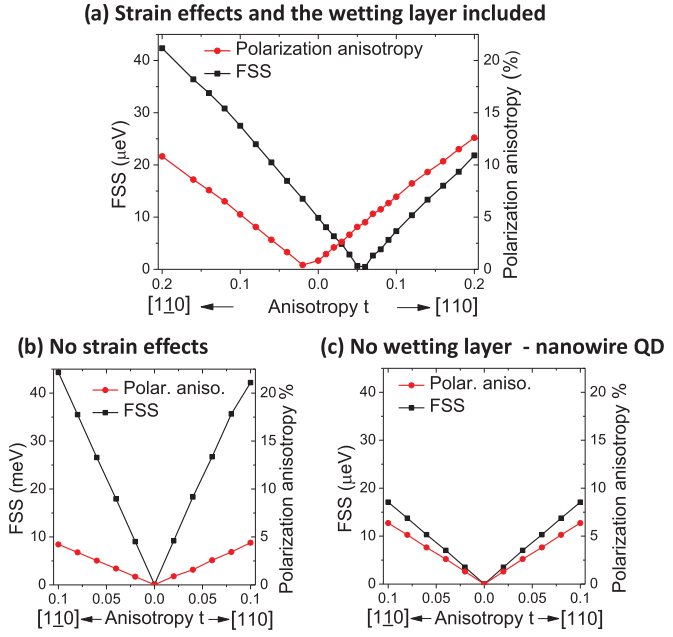

FIG. 7. (Color online) (a) The bright exciton polarization anisotropy and the FSS for the elongated disk-shaped InAs/InP QD ($h = 3$ nm, $d = 18$ nm), (b) strain effects artificially neglected, (c) strain effects included and the wetting layer neglected.

With no strain effects included [Fig. 7(b)], there is almost zero (≈0.03%) anisotropy in the emission spectra for a shape-cylindrical system, being a display of small-system asymmetry due to atomic interfaces. Notably, for a cylindrical system ($t = 0$) and strain effects neglected, the lower excitonic line is polarized along [110] (not shown here), opposite to the case with strain effects included. This reveals a different character of the FSS due to the lattice geometry and strain. For disk-shaped InAs/InP QDs, strain effects not only increase significantly the magnitude of the FSS for a shape-cylindrical system, but also reverse the polarization of the bright excitonic doublet. Thus, despite low 3% magnitude in InAs/InP systems, the strain plays an essential role for both qualitative and quantitative character of the FSS. This is an important statement as InAs/InP QDs are widely considered "low-strain" quantum dots as opposed to "highly strained" InAs/GaAs nanosystems.

For a QD without wetting layer (nanowire QD), there is no anisotropy due to high-quantum-dot symmetry [Fig. 7(c)]. In both Figs. 7(b) and Fig. 7(c) (i.e., either no strain effects or no wetting layer included), the polarization anisotropy is correlated with the increasing FSS due to the increased shape elongation, the low-energy excitonic line has higher intensity, and it is polarized along the QD elongation axis (not shown here).

B. Lens-type QDs

To study further the role of strain, I also carried out calculation for the "standard" lens-shaped InAs/InP and InAs/GaAs QDs. For the sake of comparison with the EPM calculations,[36,61] these cylindrical QDs have a diameter of 25 nm and a height of 3.5 nm [Fig. 1(b)]. Both quantum dots are located on a 0.6-nm-thick wetting layer. Despite the cylindrical shape of lens-type quantum-dot base, due to pronounced shape curvature, these QDs reveal large FSS: 43 μeV for the InAs/InP system and 57.8 μeV for the InAs/GaAs system. Importantly, these values are systematically larger than the values reported by the empirical pseudopotential method (EPM) calculations,[19] i.e., 12.9 μeV for the InAs/InP system and as small as 2.6 μeV for the InAs/GaAs system. Although recently the effects of the atomic ordering[27] have been suggested as the explanation for large FSS values typically observed experimentally, using our approach I predict pronounced (> 40 μeV) FSS without the necessity of accounting for "atomic ordering."

When strain effects are neglected, the FSS for the lens-shaped InAs/InP QD drops significantly to 1.6 μeV. This value is notably larger than practically zero FSS for the unstrained disk-shaped InAs/InP QDs due to the curved shape of lens-type QD (large-shape-inversion asymmetry). Nevertheless, again this demonstrates that strain is an essential contribution to the FSS for InAs/InP quantum dots.

For the InAs/GaAs QD, the FSS drops to -7.9 μeV when strain effects are neglected, where the minus sign marks the reversal of the excitonic polarization. As the InAs dot and GaAs matrix share the same anions (As) and the ground hole state is built mainly from As atomic p orbitals, one can speculate that this reversal is due to increased hole wave localization at the interface.[25]

The FSS has been recently decomposed[25] into the "intrinsic FSS", which is nonzero even in a cylindrical quantum dot and the "shape-asymmetric FSS" due to deviation from the macroscopic shape symmetry. In this paper, I further divide the "intrinsic FSS" into the contribution from the unstrained lattice (atomic) interfaces, i.e., 1.6 μeV for InAs/InP and -7.9 μeV for InAs/GaAs lens-type QDs, and the contribution due to the strain being roughly proportional to the strain magnitude (lattice mismatch), i.e., ≈40 μeV for InAs/InP and ≈66 μeV for InAs/GaAs lens-type QDs.

C. Alloying

In the following, I return to disk-shaped ('indium-flushed"[54]) QDs. So far, I have shown results obtained without altering the perfect symmetry of the underling zinc-blende crystal lattice. Alloying may affect QD spectra and should be accounted for.[62,63] A notable example includes thermally annealed quantum dots[5] that reveal reduced FSS and increased exciton energy due to migration of the barrier material into the quantum-dot area. Understanding of the FSS reduction in annealed quantum dots typically focuses on quantum-dot-shape symmetry[4] and explains it in terms of "symmetrizing of the in-plane confinement potential"[5] due to thermally activated diffusion and making effectively the quantum-dot shape more cylindrical. Whereas not disagreeing with the above statement, in the following I will show that the reduction of lattice asymmetry due to random fluctuations leads by itself to the FSS reduction even for shape elongated quantum dots. To illustrate that, Fig. 8(a) shows the evolution of

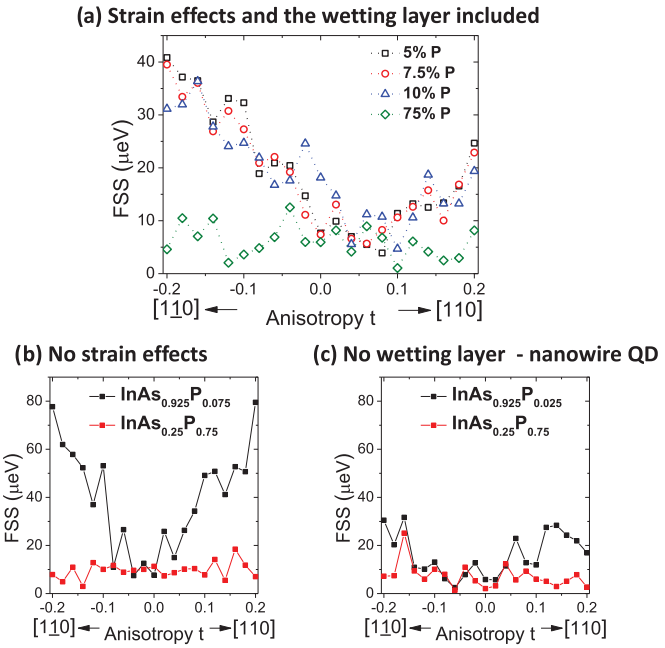

FIG. 8. (Color online) (a) The bright exciton FSS for the elongated disk-shaped $InAs_{1-x}P_x$ (alloyed) QD ($h = 3$ nm, $d = 18$ nm) and different QD compositions (phosphorous in the QD content): $InAs_{0.95}P_{0.05}$ (boxes/black), $InAs_{0.925}P_{0.075}$ [circles (red)], $InAs_{0.9}P_{0.1}$ [triangles (blue)], $InAs_{0.25}P_{0.75}$ [diamonds (green)]; (b) strain effects artificially neglected; (c) strain effects included and the wetting layer neglected.

the bright exciton splitting as a function of the QD-shape deformation for alloyed $InAs_{1-x}P_x$ quantum dots of the same (disk) shape and size, but different composition. Again, the QD height is 3 nm and the diameter is 20.6 nm. Different lines/symbols correspond to different phosphorous (P) content in the quantum dot. At the small level of alloying [up to $P \approx 10\%$ the FSS distribution resembles that from Fig. 4(a) with characteristic minimum for the [110] elongated quantum dot, however, noticeable fluctuations (to some degree proportional to P) due to alloy randomness are clearly visible. Although, in general, structural imperfections impose limits on the FSS reduction,[20] one can notice that shape elongation can still reduce significantly the FSS, even in the alloyed case. Figure 8(a) shows additionally that even for highly elongated (and thus "asymmetric in-plane confinement potential") the FSS can be significantly reduced provided a sufficiently high level of alloying (e.g., $InAs_{0.25}P_{0.75}$). The FSS reduction due to alloying in elongated quantum dots is also observed should strain effects be neglected [Fig. 8(b)] and for the case with the wetting layer removed [Fig. 8(c)]. Special attention should be paid to the latter case [Fig. 8(c)]. In this instance, quantum dots have high (D_{2d}) shape symmetry with the vertical inversion (shape) symmetry operation present, whereas the overall (shape and lattice) quantum-dot symmetry is low (C_1) and thus reduced by the alloying lattice. Figure 8(c) shows that relatively low alloying ($P = 7.5\%$) is sufficient to reduce the FSS due to shape elongation when no wetting layer is present, at least for $|t| < 0.1$, and that the FSS is comparable for very low ($P = 7.5\%$) and very high ($P = 75\%$) levels of alloying. This further confirms that quantum dots without wetting layer, such as nanowire quantum dots, are natural candidates for efficient entangled-photon generation.[19] In all considered cases at a sufficiently high level of alloying, the FSS fluctuations due to alloying dominate over extrinsic/intrinsic contributions. The FSS reduction due to alloying can not be thus explained only by symmetrizing of the in-plane confinement due to diffusion or the reduction of strain due to quantum-dot/matrix material intermixing. Therefore, further studies of lattice fluctuation effects on excitonic properties seem to be necessary. One can conclude this part by emphasizing that growth optimization techniques allowing for the control of the quantum-dot shape and composition could in principle be used to tailor the FSS, however, due to lattice randomness, selection of samples with particular low FSS may be necessary[6] unless dynamic approaches[15] for the FSS control can be utilized.

In conclusion, it has been shown that strain effects are predominantly responsible for the magnitude of the intrinsic FSS. It has also been demonstrated that the presence of the wetting layer in the self-assembled quantum dots is another key contribution to the FSS. The role of the quantum-dot-shape elongation has been investigated and it has been shown that for certain cases the bright exciton splitting can be significantly reduced. The shape anisotropy ratio, for which the FSS reduction occurs, has been found to vary with the quantum-dot size and smaller-diameter quantum dots having a larger anisotropy. It has been demonstrated that the polarization anisotropy of the excitonic emission is not simply correlated with the FSS and also that there is a spectral range when the polarization is anticorrelated with the elongation direction: the lower excitonic line follows the shorter (minor) axis of an elongated quantum dot. The FSS in cylindrical disk-shaped quantum dots has been found to be proportional to quantum-dot height and inversely proportional to quantum-dot diameter. It has been shown that the empirical tight-binding method predicts systematically much larger intrinsic FSS especially for lens-shaped, self-assembled dots and that the alloying effects play an essential role in realistic InAs/InP quantum dots.

ACKNOWLEDGMENTS

The author acknowledges support from the Foundation for Polish Science, Homing Plus Programme, cofinanced by the European Union within the European Regional Development Fund. The author would like to thank P. Hawrylak and E. S. Kadantsev for stimulating discussions and help with the manuscript.

*mzielin@fizyka.umk.pl

[1] N. Gisin, G. Ribordy, W. Tittel, and H. Zbinden, Rev. Mod. Phys. **74**, 145 (2002).

[2] J. Chen, J. B. Altepeter, M. Medic, K. F. Lee, B. Gokden, R. H. Hadfield, S. W. Nam, and P. Kumar, Phys. Rev. Lett. **100**, 133603 (2008).

[3] O. Benson, C. Santori, M. Pelton, and Y. Yamamoto, Phys. Rev. Lett. **84**, 2513 (2000).

[4] M. Bayer, G. Ortner, O. Stern, A. Kuther, A. A. Gorbunov, A. Forchel, P. Hawrylak, S. Fafard, K. Hinzer, T. L. Reinecke, S. N. Walck, J. P. Reithmaier, F. Klopf, and F. Schafer, Phys. Rev. B **65**, 195315 (2002).

[5] W. Langbein, P. Borri, U. Woggon, V. Stavarache, D. Reuter, and A. D. Wieck, Phys. Rev. B **69**, 161301(R) (2004); R. J. Young, R. M. Stevenson, A. J. Shields, P. Atkinson, K. Cooper, D. A. Ritchie, K. M. Groom, A. I. Tartakovskii, and M. S. Skolnick, *ibid.* **72**, 113305 (2005).

[6] N. Akopian, N. H. Lindner, E. Poem, Y. Berlatzky, J. Avron, D. Gershoni, B. D. Gerardot, and P. M. Petroff, Phys. Rev. Lett. **96**, 130501 (2006).

[7] R. Hafenbrak, S. M. Ulrich, P. Michler, L. Wang, A. Rastelli, and O. G. Schmidt, New J. Phys. **9**, 315 (2007).

[8] G. Juska, V. Dimastrodonato, L. O. Mereni, A. Gocalinska, and E. Pelucchi, Nat. Photonics **7**, 527 (2013).

[9] K. Kowalik, O. Krebs, A. Lematre, S. Laurent, P. Senellart, P. Voisin, and J. A. Gaj, Appl. Phys. Lett. **86**, 041907 (2005).

[10] A. J. Bennett, M. A. Pooley, R. M. Stevenson, M. B. Ward, R. B. Patel, A. Boyer de la Giroday, N. Sköld, I. Farrer, C. A. Nicoll, D. A. Ritchie, and A. J. Shields, Nat. Phys. **6**, 947 (2010).

[11] R. M. Stevenson, R. J. Young, P. Atkinson, K. Cooper, D. Ritchie, and A. Shields, Nature (London) **439**, 179 (2006); R. M. Stevenson, R. J. Young, P. See, D. G. Gevaux, K. Cooper, P. Atkinson, I. Farrer, D. A. Ritchie, and A. J. Shields, Phys. Rev. B **73**, 033306 (2006); B. D. Gerardot, S. Seidl, P. A. Dalgarno, R. J. Warburton,

D. Granados, J. M. Garcia, K. Kowalik, O. Krebs, K. Karrai, A. Badolato, and P. M. Petroff, Appl. Phys. Lett. **90**, 041101 (2007).
[12]A. Muller, W. Fang, J. Lawall, and G. S. Solomon, Phys. Rev. Lett. **101**, 027401 (2008).
[13]S. Seidl, M. Kroner, A. Högele, K. Karrai, R. J. Warburton, A. Badolato, and P. M. Petroff, Appl. Phys. Lett. **88**, 203113 (2006); F. Ding, R. Singh, J. D. Plumhof, T. Zander, V. Krapek, Y. H. Chen, M. Benyoucef, V. Zwiller, K. Dorr, G. Bester, A. Rastelli, and O. G. Schmidt, Phys. Rev. Lett. **104**, 067405 (2010).
[14]G. W. Bryant, M. Zielinski, Natalia Malkova, J. Sims, W. Jaskolski, and J. Aizpurua, Phys. Rev. Lett. **105**, 067404 (2010).
[15]R. Trotta, E. Zallo, C. Ortix, P. Atkinson, J. D. Plumhof, J. van den Brink, A. Rastelli, and O. G. Schmidt, Phys. Rev. Lett. **109**, 147401 (2012).
[16]T. Takagahara, Phys. Rev. B **62**, 16840 (2000).
[17]E. Kadantsev and P. Hawrylak, Phys. Rev. B **81**, 045311 (2010).
[18]M. Zielinski, Phys. Rev. B **88**, 115424 (2013).
[19]R. Singh and G. Bester, Phys. Rev. Lett. **103**, 063601 (2009).
[20]R. Singh and G. Bester, Phys. Rev. Lett. **104**, 196803 (2010).
[21]J. Wang, M. Gong, G.-C. Guo, and L. He, Appl. Phys. Lett. **101**, 063114 (2012).
[22]S. Tomic and N. Vukmirovic, J. Appl. Phys. **110**, 053710 (2011).
[23]O. Marquardt, S. Schulz, Ch. Freysoldt, S. Boeck, T. Hickel, E. P. O'Reilly, and J. Neugebauer, Opt. Quantum Electron. **44**, 183 (2012).
[24]K. F. Karlsson, M. A. Dupertuis, D. Y. Oberli, E. Pelucchi, A. Rudra, P. O. Holtz, and E. Kapon, Phys. Rev. B **81**, 161307 (2010).
[25]L. He, M. Gong, C. F. Li, G. C. Guo, and A. Zunger, Phys. Rev. Lett. **101**, 157405 (2008).
[26]M. Abbarchi, C. A. Mastrandrea, T. Kuroda, T. Mano, K. Sakoda, N. Koguchi, S. Sanguinetti, A. Vinattieri, and M. Gurioli, Phys. Rev. B **78**, 125321 (2008).
[27]R. Singh and G. Bester, Phys. Rev. B **84**, 241402(R) (2011).
[28]P. N. Keating, Phys. Rev. **145**, 637 (1966); R. M. Martin, Phys. Rev. B **1**, 4005 (1970).
[29]C. Pryor, J. Kim, L. W. Wang, A. J. Williamson, and A. Zunger, J. Appl. Phys. **83**, 2548 (1998).
[30]T. Saito and Y. Arakawa, Phys. E (Amsterdam) **15**, 169 (2002).
[31]W. Jaskólski, M. Zieliński, G. W. Bryant, and J. Aizpurua, Phys. Rev. B **74**, 195339 (2006).
[32]M. Zielinski, M. Korkusinski, and P. Hawrylak, Phys. Rev. B **81**, 085301 (2010).
[33]M. Zielinski, Phys. Rev. B **86**, 115424 (2012).
[34]M. Zielinski, J. Phys.: Condens. Matter **25**, 465301 (2013).
[35]M. Zielinski, Acta Phys. Pol., A **122**, 312 (2012).
[36]M. Gong, K. Duan, Ch.-F. Li, R. Magri, G. A. Narvaez, and L. He, Phys. Rev B **77**, 045326 (2008).
[37]A. Schliwa, M. Winkelnkemper, and D. Bimberg, Phys. Rev. B **76**, 205324 (2007).
[38]M. Usman, Phys. Rev. B **86**, 155444 (2012).
[39]M. Usman, J. Appl. Phys. **110**, 094512 (2011).
[40]G. Bester and A. Zunger, Phys. Rev. B **71**, 045318 (2005).
[41]G. Bester, A. Zunger, X. Wu, and D. Vanderbilt, Phys. Rev. B **74**, 081305 (2006).
[42]D. J. Chadi, Phys. Rev. B **16**, 790 (1977).
[43]J. M. Jancu, R. Scholz, F. Beltram, and F. Bassani, Phys. Rev. B **57**, 6493 (1998).
[44]G. Onida, L. Reining, and A. Rubio, Rev. Mod. Phys. **74**, 601 (2002).
[45]S. Schulz, S. Schumacher, and G. Czycholl, Phys. Rev. B **73**, 245327 (2006).
[46]A. Franceschetti, L. W. Wang, H. Fu, and A. Zunger, Phys. Rev. B **58**, R13367 (1998).
[47]S. V. Goupalov and E. L. Ivchenko, Phys. Solid State **43**, 1867 (2001).
[48]K. Leung and K. B. Whaley, Phys. Rev. B **56**, 7455 (1997).
[49]S. Lee, L. Jönsson, J. W. Wilkins, G. W. Bryant, and G. Klimeck, Phys. Rev. B **63**, 195318 (2001).
[50]C. Delerue and M. Lannoo, *Nanostructures: Theory and Modelling* (Springer, Berlin, 2004).
[51]P. Hawrylak and M. Korkusinski, in *Single Quantum Dots: Fundamentals, Applications, and New Concepts*, edited by P. Michler, Topics in Applied Physics, Vol. 90 (Springer, Berlin, 2003).
[52]W. Sheng, S.-J. Cheng, and P. Hawrylak, Phys. Rev. B **71**, 035316 (2005).
[53]Y. M. Niquet, Phys. Rev. B **74**, 155304 (2006).
[54]Z. R. Wasilewski, S. Fafard, and J. P. McCaffrey, J. Cryst. Growth **201**, 1131 (1999).
[55]Y. M. Niquet and D. C. Mojica, Phys. Rev. B **77**, 115316 (2008).
[56]C.-H. Lin, W.-T. You, H.-Y. Chou, S.-J. Cheng, S.-D. Lin, and W.-H. Chang, Phys. Rev. B **83**, 075317 (2011).
[57]G. Bester, S. Nair, and A. Zunger, Phys. Rev. B **67**, 161306(R) (2003).
[58]C. Dion, P. Desjardins, N. Shtinkov, M. D. Robertson, F. Schiettekatte, P. J. Poole, and S. Raymond, Phys. Rev. B **77**, 075338 (2008).
[59]S. Lee, O. L. Lazarenkova, P. von Allmen, F. Oyafuso, and G. Klimeck, Phys. Rev. B **70**, 125307 (2004).
[60]W. A. Coish and J. M. Gambetta, Phys. Rev. B **80**, 241303(R) (2009).
[61]L. He and A. Zunger, Phys. Rev. B **73**, 115324 (2006).
[62]M. Gong, W. Zhang, G.-C. Guo, and L. He, Phys. Rev. Lett. **106**, 227401 (2011).
[63]G. Klimeck, F. Oyafuso, T. B. Boykin, R. C. Bowen, and P. von Allmen, Comput. Model. Eng. Sci. **3**, 601 (2002).
[64]The computational domain used for calculations in this paper corresponds to a cylindrical nanowire of diameter equal to 96 nm [Fig. 1(c)].